

Synchronised Cubli Operation

Albert Smed Sandager, Christian Mølgaard Nielsen, Ivelin Krasimirov Penchev, Jaan Moos,
Kristian Helmer Kjær Larsen, and Yuheng Wang

Section of Automation and Control, Department of Electronic Systems, Aalborg University (AAU)
Fredrik Bajers Vej 7, 9220 Aalborg East, Denmark

E-mail: [asanda17, cmni17, ipench16, jmoos20, khkl17, ywang20]@student.aau.dk

Abstract—This paper is a continuation of the work done by previous AAU student projects and verifies the possibility of synchronising start up and shut down between two Cublis. A tuned linear-quadratic-regulator (LQR)-based controller for balancing is presented, along with a start up speed controller to facilitate the synchronisation. To reduce the impact with the ground when a Cubli is turned off, two shut down procedures are considered: one braking a spinning wheel before impact, and a second applying torque to the reaction wheel while falling, thus decelerating the descent of the Cubli. To enable communication between two Cublis, a second Cubli is constructed and wireless communication hardware is installed on both systems. The 802.11/b/g/n Wi-Fi protocol is used for transferring data packets. The network experiences periodical communication dropouts and delay variations. In this paper, the communication architecture is designed as a state machine to facilitate the network implementation. Networked control is also tested on the systems, but communication delays cause instability. However, for synchronising motion between two Cublis, it has been observed that the delay is insignificant, but the synchronisation is affected by the communication dropouts. Test results verify that the two Cublis can synchronise start up without any notable delay, as well as the beginning of the shut down procedures.

I. INTRODUCTION

Inverted pendulums are a common setup for testing and demonstrating control theory. In 2012 ETH Zürich started development of a reaction-wheel-based inverted pendulum called a Cubli [1]. The 3D Cubli is an unsupported cube controlled by three perpendicular reaction wheels, as seen on Fig. 1. Before the development of the 3D Cubli, a prototype 2D Cubli was developed. It is using a single reaction wheel and it moves around a fixed bearing at the vertex of the square frame [1] as seen on Fig. 2.

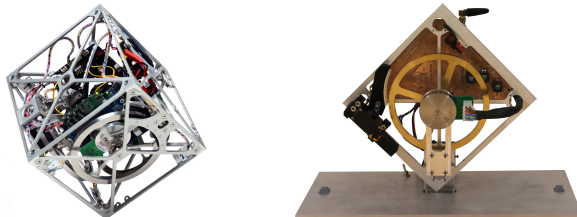


Fig. 1: The 3D Cubli from [2]. Fig. 2: AAU's 2D Cubli.

Servomotor-actuated brakes are used to allow for the necessary forces for getting the Cubli from a lying position to standing.

The team from ETH Zürich developed a dynamic model for the system and converted it into a linear state space model for designing a full state feedback controller using LQR. A method was developed for continually correcting the reference angle to compensate for a discrepancy of the balancing angle of the Cubli [1]. The development of the 3D Cubli was undertaken as described in [2] [3] [4].

Student semester projects concerning Cubli-based inverted pendulums have been going on at the section of Automation and Control at Aalborg University since 2014. The main body of work has been concerning a 2D Cubli, but a 3D Cubli is also currently being developed. This paper is a continuation of the work on the 2D Cubli, from now on just referred to as Cubli. The last semester project concerning the Cubli [5] completed the following tasks:

- 1) A linear model for the system was developed using Newtonian mechanics in accordance with the model from [1].
- 2) Model parameters were estimated through direct measurements and using the MATLAB toolkit SEN-STOOLS.
- 3) A state space model for the system was developed from the model of the system's dynamics.
- 4) Two approaches for designing a full state feedback controller were attempted: one using pole placement, and one using LQR. The LQR based controller was tested and tuned.
- 5) A complementary filter for the Inertial Measurement Unit (IMU) was developed.

In this paper, the old Cubli is modified to allow for wireless communication, and a second Cubli is produced. The novelty of this paper is the synchronisation of two Cublis and the implementation of two new shut down procedures. Additionally, improvements to the list above include new parameter estimates in the dynamic model of the Cubli, a tuned LQR-based controller, and a new start up procedure.

State-machine-based communication is set up using XBEE S6B on the two Cublis. This allows for synchronisation of the start up and shut down procedures. Finally, network control is attempted with the LQR-based controller.

In this paper, II describes the materials and methods used for achieving the above-stated improvements and III presents results of the conducted tests with their discussion. Finally, IV concludes the main findings and explores future work possibilities.

II. MATERIALS & METHODS

Before designing a controller for the system, a dynamic model is needed.

A. Dynamic Model of the System

A different approach compared to previous work done by [5] and [6] is taken to find a dynamic model of the system. A sketch of the system can be seen in Fig. 3.

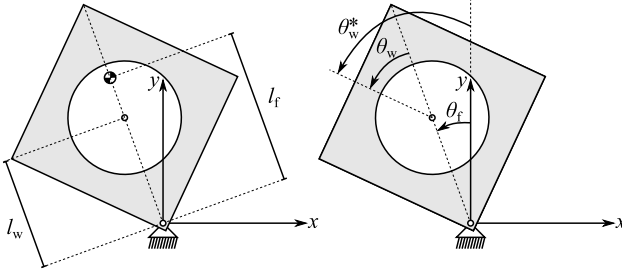


Fig. 3: A sketch of the system illustrating the angles and the two lengths l_f and l_w . The centre of mass of the frame is denoted by the \oplus symbol. Note the difference between the angles θ_w and θ_w^* .

Using the generalised coordinates $[\theta_w^*, \theta_f]^T$ a non-linear model is found using Lagrangian mechanics, where the Lagrangian L , the Rayleigh dissipation function D , and the generalised forces \mathbf{Q} are given by:

$$\begin{aligned} L &= \frac{1}{2} \cdot J_f \cdot \dot{\theta}_f^2 + \frac{1}{2} \cdot m_w \cdot l_w^2 \cdot \dot{\theta}_f^2 + \frac{1}{2} \cdot J_w \cdot \dot{\theta}_w^{*2} \\ &\quad - g \cdot (m_w \cdot l_w + m_f \cdot l_f) \cdot \cos(\theta_f) \\ D &= \frac{1}{2} \cdot b_f \cdot \dot{\theta}_f^2 + \frac{1}{2} \cdot b_w \cdot (\dot{\theta}_w^* - \dot{\theta}_f)^2 \\ \mathbf{Q} &= \begin{bmatrix} -\tau_m \\ \tau_m \end{bmatrix} \end{aligned} \quad (1)$$

where g is the gravitational acceleration, τ_m is the torque from the motor, m is the mass, J is the moment of inertia, and b is the viscous friction coefficient. The angles θ and the distances l to the centres of mass can be seen on Fig. 3. The subscripts "w" and "f" denote the reaction wheel and the frame, respectively. Using the substitution $\theta_w = \theta_w^* - \theta_f$, (1) then results in:

$$\begin{aligned} \ddot{\theta}_f &= \frac{g \cdot (m_w \cdot l_w + m_f \cdot l_f)}{J_f + m_w \cdot l_w^2} \cdot \sin(\theta_f) + \frac{-b_f}{J_f + m_w \cdot l_w^2} \cdot \dot{\theta}_f \\ &\quad + \frac{b_w}{J_f + m_w \cdot l_w^2} \cdot \dot{\theta}_w + \frac{-1}{J_f + m_w \cdot l_w^2} \cdot \tau_m \\ \ddot{\theta}_w &= \frac{-b_w}{J_w} \cdot \dot{\theta}_w + \frac{1}{J_w} \cdot \tau_m - \ddot{\theta}_f \end{aligned} \quad (2)$$

This model is then linearised around the balancing point and converted into a state space model:

$$\dot{\mathbf{x}} = \mathbf{A}\mathbf{x} + \mathbf{B}\tau_m \quad (3)$$

where:

$$\begin{aligned} \mathbf{A} &= \begin{bmatrix} 0 & 1 & 0 \\ \frac{g \cdot (m_w \cdot l_w + m_f \cdot l_f)}{J_f + m_w \cdot l_w^2} & \frac{-b_f}{J_f + m_w \cdot l_w^2} & \frac{b_w}{J_f + m_w \cdot l_w^2} \\ \frac{-g \cdot (m_w \cdot l_w + m_f \cdot l_f)}{J_f + m_w \cdot l_w^2} & \frac{b_f}{J_f + m_w \cdot l_w^2} & \frac{-b_w \cdot (J_w + J_f + m_w \cdot l_w^2)}{J_w \cdot (J_f + m_w \cdot l_w^2)} \end{bmatrix} \\ \mathbf{B} &= \begin{bmatrix} 0 \\ -\frac{1}{J_f + m_w \cdot l_w^2} \\ \frac{J_w + J_f + m_w \cdot l_w^2}{J_w \cdot (J_f + m_w \cdot l_w^2)} \end{bmatrix} \quad \text{and} \quad \mathbf{x} = \begin{bmatrix} \theta_f \\ \dot{\theta}_f \\ \dot{\theta}_w \end{bmatrix} \end{aligned} \quad (4)$$

This model is in agreement with the models derived in [1] and [5]. Using the methods also used by [1] and [5], the values for the parameters in Table I are found.

TABLE I: Estimated parameters

Symbol	Value	Unit
m_f	0.546	kg
l_f	0.0958	m
J_f	0.0067	kg · m ²
b_f	0.0036	N · m · s · rad ⁻¹
m_w	0.220	kg
l_w	0.092	m
J_w	$0.699 \cdot 10^{-3}$	kg · m ²
b_w	$1.93 \cdot 10^{-5}$	N · m · s · rad ⁻¹
g	9.816	m · s ⁻²

These parameter estimates are comparable to those found by [5]. The state space model in (4) has poles at -9.3 , -0.028 and 8.9 . The system is therefore unstable. The state space model is used for designing the controller.

B. Controller Design

As in [1] and [5] an LQR-based full state feedback controller is implemented. The LQR is the optimal gain vector \mathbf{K} that minimises the cost function:

$$f(\tau_m) = \int_0^\infty \mathbf{x}^T \mathbf{Q} \mathbf{x} + R \cdot \tau_m^2 dt, \text{ subject to: } \dot{\mathbf{x}} = \mathbf{A}\mathbf{x} + \mathbf{B}\tau_m \quad (5)$$

Resulting in the full state feedback \mathbf{K} :

$$\tau_m = -\mathbf{K} \cdot \mathbf{x} \quad \text{where: } \mathbf{K} = R^{-1} \mathbf{B}^T \mathbf{S} \quad (6)$$

where \mathbf{S} is the solution of the algebraic Riccati equation. The initial values for the \mathbf{Q} and R weighing matrices are found using Bryson's Rule [7, p. 493]. The entries $\mathbf{Q}_{i,i}$ are the weights of the response of the state \mathbf{x}_i , and R is the weight of the input to the system. The weights \mathbf{Q} and R are then tuned by increasing $\mathbf{Q}_{1,1}$ and decreasing R to decrease the settling time while allowing a small overshoot. To avoid problems with the Cubli not being perfectly balanced around the diagonal, an automatic reference angle adjustment has been implemented by [5]. Additionally, start up and shut down procedures for the system are designed.

C. Shut Down

Previously in [5], the shut down procedure was just to turn off the DC-motor and allow the Cubli to free fall. To lessen the impact, two new procedures have been developed. The first method works by accelerating the reaction wheel in the opposite direction of the fall and then actuating the brake just before impact to apply a momentary force in the opposite direction of the fall.

In the second method, torque from the motor is applied during the fall to accelerate the wheel in the direction of the fall, thus reducing the acceleration of the frame. A function for the torque with respect to the angle of the frame is developed. For this, the free body diagram in Fig. 4 is used.

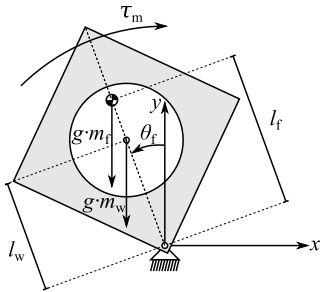


Fig. 4: Free body diagram used for developing the shut down procedure.

According to Newton's second law for rotational bodies, to reduce the acceleration by a factor α , ignoring friction, the torque from the motor is set to:

$$\tau_m = \alpha \cdot g \cdot (m_f \cdot l_f + m_w \cdot l_w) \cdot \sin(\theta_f) \quad (7)$$

The factor α is found empirically, attempting to lessen the rebound after impact.

D. Start Up

Prior to start up, the Cubli is at a resting position, lying down on its side. Before the feedback controller can balance the Cubli, it needs to get up to the balancing point, which is done by speeding up the reaction wheel and then applying the brake. A gain feedback controller for the reaction wheel's angular velocity is implemented, which allows the wheel to achieve the necessary velocity before the brake is applied.

A model for finding the necessary velocity of the reaction wheel is found as in [1]. The braking of the wheel is modelled as a completely inelastic collision between the wheel and the frame:

$$J_w \cdot \dot{\theta}_{w,b} = (J_f + J_w + m_w \cdot l_w^2) \cdot \dot{\theta}_{f,a} \quad (8)$$

where the subscripts "a" and "b" refer to after and before the collision, respectively. Ignoring friction, the movement from the resting position to the balancing point is then modelled as a change in kinetic energy ΔT being equal to a change in potential energy ΔV from the initial position of the frame $\theta_{f,i}$:

$$\Delta T = \Delta V \quad (9)$$

where:

$$\Delta T = \frac{1}{2} \cdot (J_f + J_w + m_w \cdot l_w^2) \cdot \dot{\theta}_{f,a}^2 \quad (10)$$

$$\Delta V = g \cdot (m_f \cdot l_f + m_w \cdot l_w) \cdot (\cos(0) - \cos(\theta_{f,i}))$$

Combining (8) with (9) yields:

$$\dot{\theta}_{w,b} = \frac{J_f + J_w + m_w \cdot l_w^2}{J_w} \cdot \sqrt{\frac{2 \cdot g \cdot (m_f \cdot l_f + m_w \cdot l_w)}{J_f + J_w + m_w \cdot l_w^2} \cdot (1 - \cos(\theta_{f,i}))} \quad (11)$$

From this, the required initial velocity of the wheel can be computed.

E. Synchronised Cubli Motion

Using the start up method described in subsection II-D the start up instant of time of one Cubli depends solely on the instant of time of applying the brake. Therefore, the problem of synchronising the start up of two Cublis narrows down to synchronising the braking, once both reaction wheels have reached their required velocities.

Regarding synchronised shut down, the solution presented in this paper aims only at initiating the shut down procedures synchronously, rather than ensuring simultaneous impact with the ground.

The following list presents the desired behaviour of the two Cublis regarding their synchronised motion:

- 1) Motors must be off until both systems are switched on.
- 2) Both reaction wheels must have reached their start up velocity before applying the brake.
- 3) Braking must be synchronized, subject to communication delays.
- 4) If a Cubli falls because of disturbances, the fallen Cubli must get up.
- 5) If both Cublis fall due to disturbances, they must perform a synchronised start up.
- 6) If at least one system is turned off, both Cublis must begin their shut down procedures.

To achieve the above-mentioned functionalities, a communication network is designed and implemented.

F. Communication Setup and Infrastructure

The physical setup consists of an Arduino MKR Vidor 4000 as the main processing unit, where different sensors have been attached as can be seen in Fig. 6. For communication between the Cublis, an XBEE S6B module is implemented on each of them, using the 802.11/b/g/n WiFi protocol with a bandwidth of 320 kbps. The structure of the payload of the packet for communication is illustrated in Fig. 5.

1 Byte	4 Byte	4 Byte	4 Byte	4 Byte
CMD	Angular Error	Velocity of Frame	Velocity of Wheel	Current

Fig. 5: Communication packet payload structure. The total size of the payload is 17 bytes.

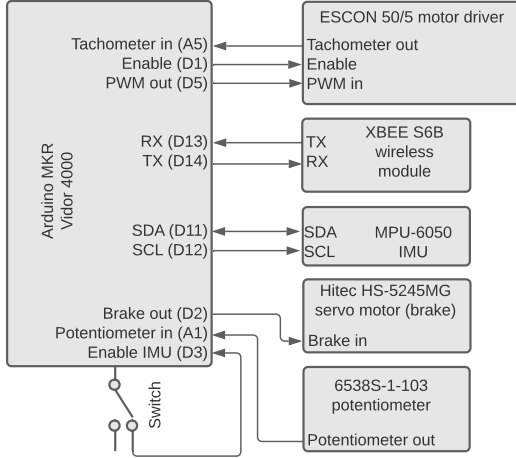


Fig. 6: Diagram of the physical setup.

The chosen architecture for the communication implementation is a state machine. To fulfil the functionalities listed in II-E, the state machine in Fig. 7 is developed and implemented.

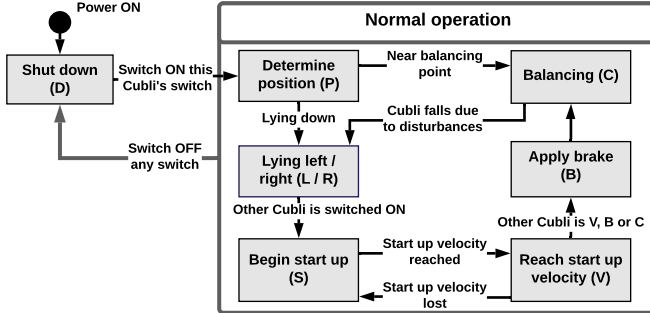


Fig. 7: State machine structure.

G. Networked Control

For studying the effects of communication on the controller, an alternative application is developed, where the network is used in the control loop. After start up, the Cublis stabilise using the regular control scheme. Then the Cublis begin calculating each other's motor torque as seen in Fig. 8. One Cubli is transmitting its measurement data to the other Cubli, which is then computing the control input of the first Cubli. It transmits the computed control signal back so it can be applied by the first Cubli. Note that this test setup is not part of the standard Cubli operation described by Fig. 7.

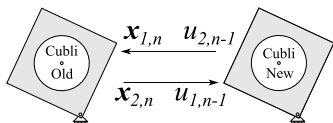


Fig. 8: Networked control diagram. The systems state is denoted by \mathbf{x} and the control input is u at samples n and $n - 1$.

III. RESULTS

A number of experiments have been conducted for designing and testing the system described in the previous section.

A. Controller Results

Using Bryson's Rule, the following values for Q and R are found:

$$Q_{i,i} = (\max(\mathbf{x}_i))^{-2}$$

$$Q = \begin{bmatrix} \left(\frac{\pi}{4} \text{ rad}\right)^{-2} & 0 & 0 \\ 0 & \infty^{-2} & 0 \\ 0 & 0 & \left(628 \frac{\text{rad}}{\text{s}}\right)^{-2} \end{bmatrix} = \begin{bmatrix} 1.62 & 0 & 0 \\ 0 & 0 & 0 \\ 0 & 0 & 2.53 \cdot 10^{-6} \end{bmatrix}$$

$$R = (\max(\tau_m))^{-2} = (0.251 \text{ Nm})^{-2} = 15.8 \quad (12)$$

This results in the following full state feedback controller K using (4):

$$K = [-1.58 \quad -1.66 \cdot 10^{-1} \quad -4.20 \cdot 10^{-4}] \quad (13)$$

Which results in the closed-loop poles of the system becoming -0.522 and $-9.34 \pm 1.99 \cdot j$.

The weights Q and R are tuned by multiplying $Q_{1,1}$ by a factor of 100 and R by a factor of 0.05 to get a satisfactory result, as described in II-B. The full state feedback controller becomes:

$$K = [-15.1 \quad -0.529 \quad -1.81 \cdot 10^{-3}] \quad (14)$$

The new closed-loop pole locations are -0.127 and $-29.7 \pm 28.1 \cdot j$. These two controllers, as well as the one from [5], are then tested. This is done to investigate the transient responses of the different controllers. The tests are performed by resting the Cubli at an angle, and then turning on the controller. This results in $\dot{\theta}_f(0) = \dot{\theta}_w(0) = 0$ and $\theta_f(0) \approx 0.17 \text{ rad}$. Fig. 9 shows test results comparing the responses of the different controllers.

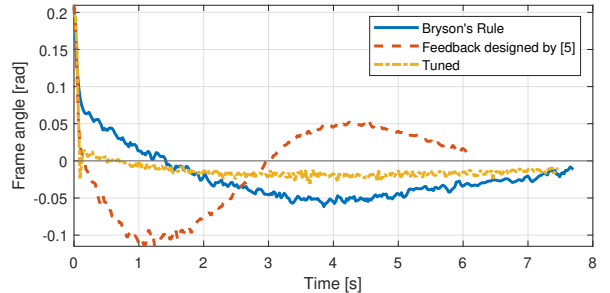


Fig. 9: Test data using Bryson's rule (13), the old controller from [5], and the tuned one (14).

The response of the tuned LQR-based controller is improved compared to the previous one found by [5]. The overshoot has been decreased as well as the settling time. It should be noted that none of the controllers in the test results from Fig. 9 manages to get to 0 rad. This is presumably caused by the Cubli not being perfectly balanced along the diagonal of the frame.

Following the design of the new controller, the start up and shut down procedures were tested and implemented.

B. Start Up Results

The following tests are performed to find suitable start up velocities for the Cublis to reach their balancing point. The frame of the Cubli initially lies down, thus $\theta_{f,i} = \frac{\pi}{4}$. Equation (11) yields the initial estimate:

$$\dot{\theta}_{w,b} = 143 \text{ rad} \cdot \text{s}^{-1} \approx 1366 \text{ RPM} \quad (15)$$

The initial reaction wheel velocities in Table II were found empirically using a bisection-based approach with (15) as a starting point. If the frame does not reach the balancing point, the reaction wheel velocity is increased, and if it overshoots, the reaction wheel velocity is decreased.

TABLE II: The old, modified Cubli and new Cubli's start up velocities

Cubli	Left side	Right side
Old, modified	1400 RPM	1540 RPM
New	1320 RPM	1597 RPM

The small differences between left and right are due to the Cubli being unbalanced. On average, the values found experimentally are higher than the estimate. This is due to the lack of friction in the model and the collision not being perfectly inelastic.

C. Shut Down Results

Experiments have been conducted to find which of the two methods reduce the impact with the ground the most. A satisfactory response of deceleration method is achieved when the slow down factor $\alpha = 1.0$. Note that according to the model, the Cubli would not move with this value, but the model is imperfect. Fig. 10 illustrates the test results comparing free fall to braking before impact and deceleration.

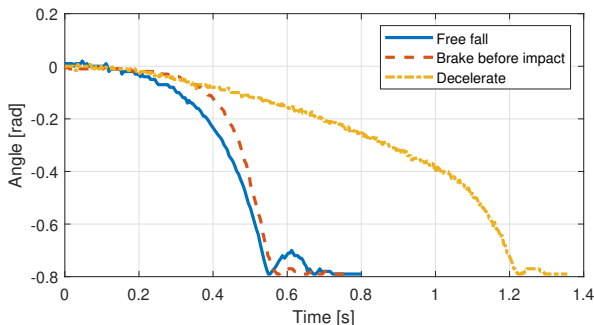


Fig. 10: Test results comparing the two new shut down methods and free fall.

Both new methods for the shut down reduce the impact with the ground, indicated by the smaller amplitude of the spike after impact. The braking before impact method for shut down is more unreliable as it depends on the conditions of the system before the shut down. Meanwhile, the deceleration method is more robust with regards to the initial conditions.

Following the design and testing of the controller locally on each Cubli, the communication is implemented and tested.

D. Delay Results

To evaluate the performance of the network, the delay in the system is examined. This is tested by transmitting several thousand packets and recording the delay time for each packet from peer to peer. The results can be seen in Fig. 11.

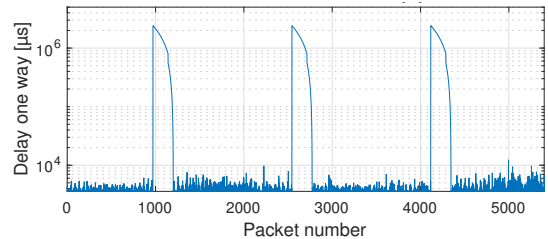


Fig. 11: Test results for delay measurements.

In Fig. 11 periodical delay spikes can be seen. The reason for these delay spikes on the communication channel is currently unknown, but presumed to be caused by the hardware itself. Different packet sizes and packet rates have been tested, but the delay spikes remain. However, using other wireless communication modules such as the HM-10 Low Energy Bluetooth module, it is possible to eliminate the delay spikes. Unfortunately, the HM-10 modules are considered too slow with a roundtrip delay of 56 ms, and are therefore not suitable for this project. This supports the presumption, that the XBEE S6B modules are the cause of the issue.

Omitting the delay spikes, the delay has a mean of 3.8 ms and a standard deviation of 0.33 ms.

After estimating the mean communication delay, a requirement for maximum delay between two synchronised systems must be specified. This defines whether the system is capable of synchronising the Cublis over the designed network.

E. Synchronised Motion Results

Before testing the synchronisation of the two Cublis, an acceptable limit first can be determined using the following experiment: two LEDs 1 cm apart are turned on with a delay between them. The delay is changed with 1 ms increments, and a human observer has to determine which of the two LEDs is turning on first. The lower bound for the noticeable delay is found to be 25 ms. Other factors may influence the limit of noticeable delay, such as the nature of the action itself, or the distance between the actions.

To test whether the two Cublis operate synchronously, an LED is enabled on each Cubli at the time of applying the brake. A video is taken and its frames are analysed, taking into consideration the refresh rate of the video clip. Thereby, upper bounds for delay during synchronised motion can be estimated by observing the two LEDs and the interval between their enable times.

Fig. 12 shows the measurement of delay between two Cublis during synchronised start up filmed at 480 FPS.

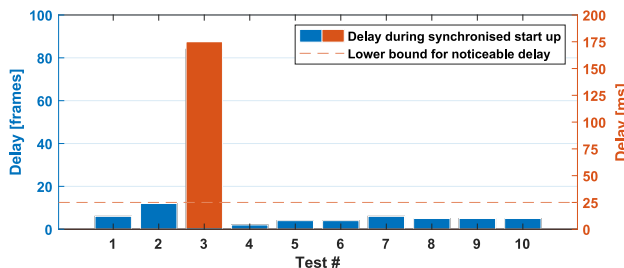


Fig. 12: Maximum delay during synchronised start up compared to the lower bound for noticeable delay.

The 3rd measurement is considerably higher than the rest. This is presumably caused by the delay spikes described in subsection III-D. The rest are all below the lower bound found in the first test from this subsection. Additionally, the minimum synchronisation delay is comparable to the mean delay from subsection III-D.

F. Networked Control Results

As mentioned in II-G, the effects of communication on the controller are examined by having the two Cublis exchange their measurement data and thereby calculating each other's control input. Results from one Cubli's position data and applied motor torque are shown in Fig. 13.

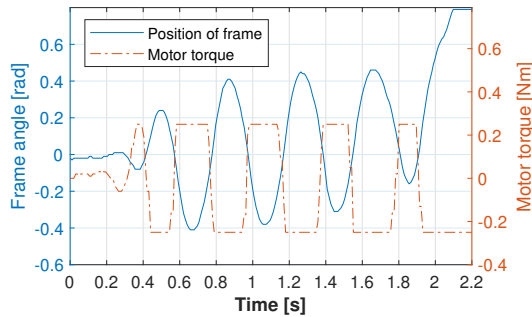


Fig. 13: Angular position of a Cubli and the motor torque received over the communication channel from the other Cubli.

As can be seen from the results, the system becomes unstable during the networked control, which causes the Cubli to fall over within a few seconds. This is presumed to be caused by the increased delay.

IV. CONCLUSION

The new method for the shut down procedure, where torque is applied to the frame during the fall, slows down the Cubli considerably and thus lessens the impact with the ground.

According to the test result in Fig. 12, the delay between the two systems is below the lower bound of 25 ms for noticeable delay, except for the third test. This large delay is presumed to be caused by periodic delay spikes in the communication network.

Although the communication channel is sufficient for synchronising the start up and shut down procedures, Fig. 13

shows that when the control input is calculated outside the system, it becomes unstable and eventually the Cubli falls to one side. This is presumed to be caused by the added delay from the communication in the control loop, as well as the potential packet losses. Normally, a Smith predictor can be implemented to handle effects of delays. However, it is not applicable for systems with unstable open-loop dynamics [8, p. 273], such as the Cubli.

Further investigation into the cause of and a solution to the delay spikes is necessary.

REFERENCES

- [1] M. Gajamohan, M. Merz, I. Thommen, and R. D'Andrea, "The cubli: A cube that can jump up and balance," in *2012 IEEE/RSJ International Conference on Intelligent Robots and Systems*, 2012, pp. 3722–3727. DOI: 10.1109/IROS.2012.6385896.
- [2] M. Muehlebach and R. D'Andrea, "Nonlinear analysis and control of a reaction-wheel-based 3-d inverted pendulum," *IEEE Transactions on Control Systems Technology*, vol. 25, no. 1, pp. 235–246, 2017. DOI: 10.1109/TCST.2016.2549266.
- [3] M. Gajamohan, M. Muehlebach, T. Widmer, and R. D'Andrea, "The cubli: A reaction wheel based 3d inverted pendulum," in *2013 European Control Conference (ECC)*, 2013, pp. 268–274. DOI: 10.23919/ECC.2013.6669562.
- [4] M. Muehlebach, G. Mohanarajah, and R. D'Andrea, "Nonlinear analysis and control of a reaction wheel-based 3d inverted pendulum," in *52nd IEEE Conference on Decision and Control*, 2013, pp. 1283–1288. DOI: 10.1109/CDC.2013.6760059.
- [5] J. S. Knudsen, L. Røjkjær-Jensen, M. J. Riisager, G. D. Dimitrov, K. Turek, and M. H. Pedersen, "Aau3 - self balancing cube," AAU Student Report, 2019.
- [6] J. S. Knudsen, L. Røjkjær-Jensen, and M. J. Riisager, "Cubli - self balancing cube," AAU Student Report, 2019.
- [7] G. F. Franklin, J. Powell, and A. Emami-Naeini, *Feedback control of dynamic systems*, 7th ed. Pearson, 2015, ISBN: 9780133496598.
- [8] K. Åström and T. Häggglund, *Advanced PID Control*. ISA-The Instrumentation, Systems, and Automation Society, 2006, ISBN: 9781556179426. [Online]. Available: <https://www.isa.org/products/advanced-pid-control>.